Published in final edited form as:
Biomaterials. 2009 February ; 30(5): 939–950. doi:10.1016/j.biomaterials.2008.10.012.

Gene delivery *in vitro* and *in vivo* from bioreducible multilayered polyelectrolyte films of plasmid DNA

Jenifer Blacklock[a,b], **Ye-Zi You**[a,#], **Qing-Hui Zhou**[a], **Guangzhao Mao**[c], and **David Oupický**[a,*]

a*Department of Pharmaceutical Sciences, Wayne State University, Detroit, MI 48202, USA*

b*Department of Biomedical Engineering, Wayne State University, Detroit, MI 48202, USA*

c*Department of Chemical Engineering and Materials Science, Wayne State University, Detroit, MI 48202, USA*

Abstract

Layer-by-layer (LbL) films were assembled on flexible stainless steel substrate using plasmid DNA and reducible hyperbranched poly(amido amine) (RHB) polycation. The films were characterized by XPS and their disassembly in reducing conditions confirmed by ellipsometry. Fibroblast and smooth muscle cell attachment and proliferation on DNA/RHB films were indistinguishable from those on control DNA/poly(ethylenimine) (PEI) films. *In vitro* transfection activity was evaluated using reporter plasmids encoding for secreted alkaline phosphatase (SEAP) and green fluorescent protein (GFP). DNA/RHB films showed higher and longer lasting transfection activity than control DNA/PEI films using SEAP plasmid. Using GFP plasmid revealed that DNA/RHB films transfected almost the entire cell population growing on the films. *In vivo* transfection activity was evaluated by subcutaneously implanting a stainless steel substrate coated with the DNA/RHB films containing SEAP plasmid DNA and measuring the levels of SEAP secreted into the blood circulation of rats. It was found that the plasma levels of SEAP peaked at ~160 ng SEAP/mL five days post-implantation.

1. INTRODUCTION

Methods that offer controlled local delivery of DNA play significant role in tissue engineering [1,2] and in the development of localized gene therapy approaches [3,4]. In particular, surface-mediated delivery of DNA from thin films and coatings appears to be a promising approach to improve localized transfection activity due to the potential to maintain elevated concentrations of DNA within the local extracellular microenvironment [5-11]. Despite the recent advances, progress toward the development of localized gene therapies remains limited.

Layer-by-layer (LbL) assembly of thin multilayered polyelectrolyte films provides convenient control over the incorporation of DNA and other nucleic acids on the surface of a variety of implantable materials, biomedical devices, and tissue engineering scaffolds. The LbL assembly offers number of advantages compared to other methods of localized delivery of DNA. The method does not require the use of organic solvents and allows precise control over DNA loading. In addition, LbL assembly has the potential to achieve highly sophisticated

*Corresponding author: Tel.: +1 313 993 7669; fax: +1 313 577 2033. *E-mail address:* oupicky@wayne.edu.
#Current address: Department of Polymer Science and Engineering, University of Science and Technology of China, Anhui, Hefei, 230026, P. R. China

programmable control of gene delivery by incorporating different DNA plasmids into different layers of the film [3,12].

The LbL films are usually highly stable due to the polyvalent nature of the electrostatic interactions and their disassembly requires extreme conditions incompatible with physiological environment [13]. Successful use of DNA-containing films for gene therapy requires disassembly of the LbL films under physiologically relevant conditions [14]. Although number of strategies suitable for disassembly of LbL films have been reported in recent years [15], the approaches to the release of DNA usually rely on hydrolytically or enzymatically degradable polycations [16,17].

It was proposed that extracellular reducing microenvironment can support reduction of LbL films upon cell attachment and act as an effective trigger of film disassembly [18]. Whereas the reducing nature of the intracellular environment is a well-established fact and has been widely exploited in drug and gene delivery [19,20] and disassembly of LbL films [21-23], the reducing microenvironment of the plasma membrane received considerably less attention. To our knowledge, there has been only one report describing an attempt to utilize cell membrane thiols to improve gene delivery by increasing cellular uptake of DNA [24]. Whether the reducing potential of the plasma membrane is sufficient enough to have any significant, positive or negative, effect on the activity of LbL gene delivery films, however, still remains to be investigated.

The presence of reactive oxygen species and absence of a redox buffer means that the extracellular space is predominantly oxidizing [25]. Despite the oxidizing nature of the extracellular environment, however, the presence of redox-active thiols in numerous proteins on the cellular plasma membrane suggests that at least the microenvironment of the cell surface can support disulfide reductions [26-28]. The redox activity of the plasma membrane is closely correlated with the levels of redox enzymes at the membrane [29-31]. The maintenance of the thiol groups is mediated by the transfer or shuffling of hydrogens and electrons between the cysteine thiols of these surface proteins [32]. The total levels of redox-active thiols on the surface of cells range from ~4 to ~30 nmol/10^6 cells [32,33].

Here, we hypothesize that the reducing microenvironment of plasma membrane, rather than the intracellular reducing environment, may provide a specific stimulus for controlling the disassembly of DNA-containing LbL films fabricated with bioreducible polycations. It is expected that cell attachment will lead to cleavage of the disulfide bonds in the polycations and subsequent release of partially condensed DNA in a localized and timely manner. This study reports results of cell proliferation and *in vitro* and *in vivo* transfection studies using LbL films of DNA and RHBs coated on flexible stainless steel substrates.

2. MATERIALS AND METHODS

2.1. Materials

Branched polyethylenimine (PEI, M_w 25 kDa, Aldrich), 1-(2-aminoethyl)piperazine (AEPZ, Aldrich), 1-methylpiperazine (Aldrich), *N*,*N*'-methylenebisacrylamide (MBA, Aldrich), *N*,*N*'-cystaminebisacrylamide (CBA, Polysciences, U.S.A.), and Hoechst 33342 (Invitrogen) were used as received from the supplier. gWiz™ High-Expression GFP plasmid (6.7 kb) and gWiz™ High-Expression Secreted Alkaline Phosphatase (SEAP) plasmid (5.8 kb) were purchased from Aldevron (Fargo, ND) and used without purification. Stainless steel T304 mesh with 120 mesh woven wire with diameter 94.0 μm was purchased from TWP Inc. (Berkeley, CA). Fibroblast cells established from NIH Swiss mouse embryo (NIH-3T3) and rat aortic smooth muscle cells (SMC) were obtained from ATCC and maintained in Dulbecco's Modified Eagles Medium (DMEM) and 10% fetal bovine serum (FBS).

2.2. Polymer synthesis and characterization

Reducible hyperbranched poly(amidoamine) (RHB) was synthesized by Michael addition copolymerization of half molar ratio of a triamine AEPZ to bisacrylamide monomers (CBA and MBA). Briefly, CBA (0.260 g, 1.0 mmol) and MBA (0.308 g, 2.0 mmol) were added into a small vial containing AEPZ (0.193 g, 1.5 mmol) in methanol/water mixture (3.5 mL, 7/3 v/v). Polymerization was carried out at 50 °C for 5 days, yielding a viscous solution. Subsequently, small amount of 1-methylpiperazine was added to consume any unreacted acrylamide groups, and stirring was continued for 12 h at 50 °C. The polymer was obtained by precipitating the reaction mixture into cool acetone and dried under vacuum at room temperature.

^{1}H NMR and ^{13}C NMR spectra of RHB were recorded on a Varian spectrometer (400 MHz). The number average (M_n) and weight-average (M_w) molecular weight and polydispersity index (PDI, M_w/M_n) of the polymer were determined by size exclusion chromatography (SEC) using Shimadzu LC-10ADVP liquid chromatography equipped with CTO-10ASVP Shimadzu column oven and Polymer Labs PL gel 5 μm mixed C column. The system was equipped with multiangle light scattering detector (miniDAWN, Wyatt Technology, Santa Barbara, CA) and an interferometric refractometer (OPTILAB DSP, Wyatt Technology, Santa Barbara, CA). Sodium acetate (30 mM, pH 4.5) was used as an eluent at a flow rate of 1.0 mL/min and temperature of 35 °C. SEC data were analyzed using Astra 5.3.1.4 software from Wyatt Technology.

2.3. Preparation of LbL films

The following polyelectrolyte solutions were used in the LbL film assembly on the mesh: 1 mM RHB in 200 mM acetate buffer (pH 5.5), 1 mM PEI in 0.2 M NaCl and 0.25 g/L DNA in 100 mM sodium acetate buffer (pH = 5.5). The mesh samples were immersed first into a solution of a polycation (RHB or PEI) for 10 min. This procedure was followed by three 2-min rinses in deionized water. Following the initial layer of the polycation, 15 bilayers of plasmid DNA and RHB were deposited sequentially using the same deposition and rinse procedure and denoted as $(DNA/RHB)_{15}$ and $(DNA/PEI)_{15}$ (i.e. all films were terminated with polycation layer).

2.4. Characterization of the LbL films

Presence of $(DNA/RHB)_{15}$ films on the surface of the stainless steel mesh was confirmed by X-ray photoelectron spectroscopy (XPS). XPS data were collected using a Perkin Elmer Model 5500 spectrometer with a monochromatized Al K-alpha X-ray source (1486.6 eV) operating at 15 kV and 14 mA. The electron detector was hemispherical analyzer at 45° take-off angle. The working pressure was less than 1.0×10^{-8} torr. The spectrometer was calibrated to the Au 4f7/2 peak at 83.8 eV and the Cu 2p3/2 peak at 932.4 eV. A survey scan was acquired before each multiplex scan. All multiplex scans used pass energy of 23.5 eV with a scan step of 0.05 eV and a time/step of 60 ms. The number of sweeps per peak varied from 10 to 20.

DNA content in the LbL films deposited on the stainless steel mesh was determined by RT-PCR. Mesh samples were treated with 400 μL PCR lysis buffer (10 mM dithiothreitol (DTT), 2.0 mg/mL poly(L-aspartic acid), 0.5 mg/mL proteinase K, 1% Triton Glycerol) to release DNA from the deposited films. After 12 h incubation at room temperature, the DNA content in the lysates was measured with RT-PCR (ABI Prism® 7300) using the following cycle: 2 min at 50 °C, 10 min at 95 °C, 40 cycles for 15 s at 95 °C, and 1 min at 60 °C. The results are presented as a mean ± S.D. obtained from three mesh samples.

Ellipsometry studies were performed *in situ* to measure the film thickness over time. The measurements were performed using a silicon wafer and a phase-modulated ellipsometer

(Beaglehole Instruments, New Zealand) fixed at the angle of incidence near the Brewster angle ($\theta_B \approx 70°$). The ellipticity, $\rho = \mathrm{Im}(r_p/r_s) \mid \theta_B$ measured by the ellipsometer, where r_p and r_s which are the complex reflection amplitudes for p and s polarizations, respectively. This was next converted into film thickness using the Drude equation. The in situ experiments were performed using a 1 cm quartz cuvette that was filled with degradation solution. The substrate was placed at the bottom of the cuvette with the degradation solution and data points were automatically collected every 1 min for 14 h.

2.5. Cell attachment and proliferation

Sterilized stainless steel mesh was cut into 1-cm^2 samples, which were placed at the bottom of wells of a 12-well plate. NIH-3T3 and SMC cells were grown to 80% confluence, trypsinized, washed with phosphate-buffered saline (PBS, pH 7.0–7.2), and resuspended in DMEM. Then, 40,000 cells were placed in the well plate with the mesh and incubated in 5% CO_2 at 37 °C for 1 h. The mesh with the cells attached were then removed and placed into new wells containing fresh DMEM supplemented with 10% FBS. Cell culture medium was replaced every day by carefully washing the mesh with PBS and transferring the mesh into new well plates with 2 mL of fresh medium. Cells were imaged daily by optical and fluorescence microscopy. In some cases, the cell nuclei were labeled by incubating the mesh with 10 μM Hoechst 3342 and imaged using a Nikon TE2000-U microscope in DMEM without phenol red. The images were acquired at 37 °C using excitation/emission filters 340–380/435–485 nm. Lactate dehydrogenase (LDH) assay was used to quantify cell attachment and proliferation on the mesh using a commercial CytoTox 96® Nonradioactive Cytotoxicity Assay kit (Promega). At different time points, the mesh containing the growing cells was washed with PBS and the cells then lysed by three freeze-thaw cycles. Fifty μL of the cell lysate was diluted with 50 μL of DMEM/FBS without phenol red. The LDH substrate (50 μL) was added to each sample and incubated for 30 min in dark. Fifty μL of the stop solution was added to each sample and the absorbance was measured at 490 nm. Calibration curve (cell number vs. LDH content) was constructed using a known number of cells. The results are expressed as mean number of cells per cm^2 of the mesh ± S.D. obtained from three samples.

2.6. Scanning electron microscopy (SEM)

A Hitachi S-2400 SEM with EDAX analytical capability was used for imaging the cells on the mesh. First, cells were fixed with 2% glutaraldehyde solution in PBS at room temperature for 15–20 min. Then, cells were washed with PBS and treated with 2% osmium tetroxide in PBS for 30 min. Following this step, the sample was dehydrated with aqueous ethanol solutions of increasing concentrations (30–100% in 10% increments). Finally, the sample was dried under vacuum for 24 h. The sample was sputter coated using EffaCoater (Ernest F. Fullam) in vacuum (200 mTorr) with a sputtering current of 50–100 mA with Ag-Pb and imaged by SEM.

2.7. Transfection activity *in vitro*

Cells were seeded on the mesh coated with $(DNA/RHB)_{15}$ or $(DNA/PEI)_{15}$ LbL films using either GFP or SEAP plasmid DNA as described above. GFP expression was evaluated daily in live cells using Nikon TE2000-U fluorescence microscope (excitation/emission filters 445–485/500–545 nm) along with MetaVue software for the analysis. In selected samples, the GFP expression was analyzed by confocal microscope (Zeiss LSM-510 Meta NLO, Laser Scanning Confocal Microscope) equipped with two fluorescent detectors, a transmitted light detector, and a Zeiss Axioplan2 upright microscope with automated programmable scanning stage. GFP emission was imaged at 488 nm and nuclei stained with Hoechst3342 at 745 nm. To determine the transfection activity of the LbL films containing SEAP DNA, the cells were grown on the mesh as described above and the amount of SEAP secreted by the transfected cells into medium was measured. Two mL of medium was sampled every 24 h, replaced with fresh medium, and

immediately frozen at -80 °C until further analysis. To measure levels of SEAP reporter gene expression, 10 μL of the sample was diluted with 40 μL of the dilution buffer and heated at 65 °C for 30 min to deactivate endogenous phosphatases and then cooled on ice for another 30 min. One hundred μL of the above sample was added to a luminometer tube, mixed with 100 μL of the assay buffer (including appropriate alkaline phosphatase inhibitor), and incubated for 5 min. Then, 100 μL of reaction buffer (including CSPD® substrate) was added and the mixture was incubated for another 20 min. A single tube Sirius® luminometer (Zylux Corporation) was used to measure the luminescence with the injector set off and measurement taken for 10 s with 2 s delay time. The transfection results are expressed as mean cumulative Relative Light Units (RLU)/s ± S.D. Cumulative transfection was determined by adding up the individual RLU values obtained at the different time points. Significant differences between two groups were determined by Student's t-test. A value of $P < 0.05$ was considered statistically significant. Triplicate samples were used in all transfection experiments.

2.8. Animals

All animal experiments were approved by Wayne State University Animal Investigation Committee and followed the guidelines provided by the Association for the Assessment and Accreditation for Laboratory Animal Care International (AAALAC) and by the National Institutes of Health in Guide for the Care and Use of Laboratory Animals. Male Sprague-Dawley rats weighing ~250 g were purchased from Charles River Laboratories. The animals were allowed to acclimatize for 1 week after arrival. The animals were fed Purina laboratory chow (Ralston-Purina, St. Louis, MO) and were maintained in accordance with the standards set forth by the Animal Welfare Act. The animals were housed under controlled light with 12 h light/dark cycles and controlled temperature conditions. Rats were caged in random pairs in polycarbonate cages.

2.9. Transfection activity *in vivo*

Stainless steel mesh was cut into 2×5 cm^2 pieces and $(DNA/RHB)_{15}$ films were deposited as described above using SEAP plasmid DNA. The mesh with the LbL films was sterilized in 70% ethanol and allowed to air-dry. Next, the mesh was carefully rolled into cylinders with a diameter of ~0.2 cm. The mesh was sterilized again by 70% ethanol immediately before implantation. The sterilization procedure did not cause film loss or rearrangement. Non-coated mesh was used as control in the *in vivo* experiments. The dorsal aspect was shaved and prepped for surgery, before the rats were anesthetized with 5% isoflurane and maintained on 2.5–3% isoflurane mask. A 1 cm linear subcutaneous incision perpendicular to the spinal column at the nape of the neck was made and blunt dissection with forceps was used to create an opening for the mesh to be inserted. The mesh was placed inside the opening, the incision was closed with standards staples using a staple gun, and the animals were allowed to recover. Each rat then received a single injection of Buprenex SO (0.03 mg/kg, s.c.). The staples were removed after 5 days. Blood was collected on day 0, 1, 2, 3, 5, 7, 8, 10, 11, and 12 from the saphenous vein using a 25g needle. Each time, the withdrawn blood volume was replaced with twice the volume of i.p. saline. Two hundred μL of blood was collected each time, placed in 500 μL collection tubes coated with EDTA, and plasma was isolated by centrifugation at 3000×g for 5 min and stored at -80 °C for further analysis of SEAP expression. The rats were euthanized by CO_2 narcosis and upper thorax puncture. The mesh was surgically removed with the surrounding tissue and stored refrigerated in 10% formalin for histology analysis. The levels of SEAP in the plasma were determined as described above. The results are expressed as mean RLU ± S.D. and significant differences between two groups determined by Student's t-test. A value of $P<0.05$ was considered statistically significant. Six animals per group were used in all *in vivo* experiments.

2.10. Histology

Tissue surrounding the mesh implant, along with the mesh still intact, was preserved in 10% formalin and refrigerated. The tissue was first sectioned by slicing tissue from the skin down through to the mesh sample using a scaffold and then set in paraffin. Hematoxilin-eosin (H&E), Trichrome, and Feulgen stains were prepared for both the control mesh and the mesh with DNA/RHB films. Images were taken using an optical microscope equipped with color camera at 20× and 40× magnification.

3. RESULTS AND DISCUSSION

3.1. Synthesis and characterization of RHB

This study employs a recently established type of bioreducible poly(amido amine) polycations that have shown increased transfection levels and low cytotoxicity *in vitro* [34-36]. RHB was synthesized by Michael addition copolymerization of a triamine AEPZ with a mixture of bisacrylamide monomers (CBA: MBA = 1:2) (Scheme 1). We used hyperbranched polymers in this study because of the possibility to prepare polymers with higher molecular weights compared with similar linear polymers [34]. The higher molecular weight of hyperbranched polycations was expected to influence positively the stability and transfection activity of the DNA-containing LbL films *in vivo*. The distinct reactivity of the amines in AEPZ allows synthesis of either linear or hyperbranched polymers by simply changing the ratio of AEPZ-to-bisacrylamide monomers [37]. Using 1:2 molar ratio of AEPZ to CBA+MBA produces hyperbranched polymers, while the use of 1:1 ratio leads to the formation of linear polymers. The hyperbranched structure of the synthesized RHB was confirmed by ^{1}H- and ^{13}C-NMR and its weight-average molecular weight (M_w) was 66,000 (M_w/M_n = 1.7). This polymer was selected for the preparation of the LbL films from a series of polymers with varying content of the reducible CBA monomer due to a favorable combination of low cytotoxicity, high transfection activity, and redox sensitivity of its DNA complexes *in vitro* (data not shown). RHB efficiently condenses DNA and is reduced in the presence of mild reducing agents such as glutathione. RHB demonstrates negligible cytotoxicity in a number of tested cell lines at concentrations up to 100 μg/mL (data not shown).

3.2. Preparation and characterization of the LbL films

LbL films are typically deposited on the surface of substrates that permit easy characterization *in vitro*. Here, we assembled the films on the surface of stainless steel mesh with the diameter of the mesh wires ~80 μm. The stainless steel mesh substrate was selected for its suitability for *in vivo* experiments. Successful deposition of DNA LbL films on stainless steel was reported previously by Jewell et al using intravascular stents [38]. All experiments with the stainless steel mesh described in this study used LbL films containing 15 DNA/polycation bilayers (i.e. the films are terminated with polycation layer) based on either RHB or control PEI and containing plasmid DNA encoding either GFP or SEAP.

The surface of the mesh after the LbL deposition was examined by XPS (Fig. 1). XPS is a particularly useful analytical technique for this purpose due to its high sensitivity to the chemical structure near the surface (0.5–8 nm). The almost complete disappearance of the Fe signal combined with the presence of P and N signals in the LbL-coated mesh samples (Fig. 1b) points to the presence of DNA (P, N) and RHB (N) on the mesh surface.

In order to follow the disassembly of the DNA/RHB films induced by disulfide reduction in RHB, the degradation of the film on silicon substrate in solution was monitored by ellipsometry. The ellipsometry setup for *in situ* film disassembly monitoring has been described previously [18]. The degradation of the films was followed by monitoring the film thickness as a function of time in a phosphate buffer solution containing 20 mM DTT. Reduction of the

disulfide bonds in RHB results in the formation of short cationic residues that display lower affinity to the DNA and leads to subsequent disassembly of the DNA/RHB film. The thickness of DNA/RHB films decreased exponentially and the films disassembled almost completely over a period of 12 h (Fig. 2). On the other hand, control DNA/PEI films showed only about 10 nm decrease in their thickness over the same period of time. The disassembly rate of DNA/RHB films observed in Fig. 2 is relatively fast due to high concentration of the highly reducing DTT. One can reasonably expect that the disassembly rates will be significantly lower when the reduction of RHB is induced by the reducing microenvironment of attached cells, thereby allowing longer duration of the sustained release of DNA.

The amount of DNA deposited on the mesh was quantified by RT-PCR after complete disassembly of the films. We found that $(DNA/RHB)_{15}$ films contained 826 ± 85 ng DNA/cm^2 mesh (n=3), corresponding to an average DNA content of 55 ng per layer. Material content in individual layers of LbL films is influenced by the deposition conditions and choice of polyelectrolytes. The amount of DNA in the DNA/RHB films falls within the broad range reported previously. For example, Meyer et al. found that a single layer of DNA/PEI contained 22.5 ng DNA/cm^2 [39], while Jewell et al. reported values over 300 ng DNA/cm^2 for LbL films based on poly(β-amino ester)s [9,38].

3.3. Cell proliferation

Attachment and proliferation of NIH-3T3 and SMC cells on $(DNA/RHB)_{15}$ and $(DNA/PEI)_{15}$ films deposited on stainless steel mesh were investigated using LDH assay, optical microscopy, and SEM. The cells were seeded on mesh coated with the LbL films and maintained in standard tissue culture polystyrene plates in 5% CO_2 atmosphere and 37 °C. The mesh rested lightly on the bottom of the wells but did not become attached to the surface as the cells grew. The mesh was moved to a new well every day during replacement of culture media to eliminate any influence of cells growing on the surface of the wells. The number of cells attached to the steel mesh at different time points after seeding was determined by measuring the content of LDH in cell lysate obtained from the mesh (Fig. 3). The results confirm that both NIH-3T3 and SMC readily attach and grow on both $(DNA/RHB)_{15}$ and control $(DNA/PEI)_{15}$ films. No significant differences in the rate of cell growth were observed between the two types of LbL films tested. The fact that no differences in cell proliferation were observed between RHB- and PEI-based films suggests that there was no significant difference between the toxicity of the two films. In comparison, when cytotoxicity was tested using solutions of the two polycations, PEI exhibited significantly higher toxicity (IC50 ~10 μg/mL) than RHB (IC50 >100 μg/mL). The observation that immobilized polycations are significantly less cytotoxic is not surprising given the mechanism of polycation-induced toxicity. However, the process of gene delivery from LbL films requires DNA, and therefore polycations too, to be released from the surface, thus exposing cells to the more toxic soluble polycations. In addition, because of the inefficient disassembly of PEI-based films, only negligible toxicity related to soluble PEI is observed. As expected, the growth rate of the NIH-3T3 fibroblasts was faster than the growth rate of the SMCs. There were ~42,000 NIH-3T3 cells/cm^2 present after 8 days of growth on $(DNA/RHB)_{15}$, compared to only ~19,200 SMC/cm^2. The initial attachment of cells to the non-coated mesh was negligible compared to the attachment to the mesh coated with the films, suggesting higher affinity of cells to the positively charged DNA/polycation films compared to the negatively charged stainless steel surface [40].

The growth pattern of the NIH-3T3 cells on the mesh coated with DNA/RHB films was visualized over time by optical microscopy in a 7 day study (Fig 4). Because of the nontransparent nature of the steel wires only cells growing in spaces between the mesh wires could be observed. The first signs of cell proliferation in the mesh holes are apparent on day

2. The initial growth pattern indicates that cells first grow on and near the stainless steel frame whose surface was covered by the LbL films. The cells are seen to propagate toward the center of the mesh opening and by day 7 they fill the empty spaces in the mesh almost completely. As indicated above, the mesh samples were taken out of the well plates with minimum disturbance every day and placed in a new well plate with fresh medium. The fact that the cells were not disturbed during the transfer indicates that they formed a tightly packed network attached to the mesh with no support from the well plate. Similar, but much slower, initial growth pattern was observed for SMC growing on $(DNA/RHB)_{15}$ films. Representative image of SMC cells on day 6 with nuclei labeled with Hoechst 3342 dye for improved visibility is shown in the last panel of Fig. 4. The SMCs were predominantly located near the edge of the frame. Finally, SEM images showed the cell network intertwined on the surface of the mesh wire and throughout the mesh holes and provide a clear representation of the 3-dimensional networks after 6 days of cell growth (Fig. 5).

3.4. *In vitro* transfection

Transfection activity mediated by the LbL films on the surface of steel mesh was evaluated using SEAP and GFP reporter plasmids in NIH-3T3 and SMC. We used mesh coated with $(DNA/RHB)_{15}$ and $(DNA/PEI)_{15}$. Transfection activity of the LbL films containing SEAP-DNA was determined by measuring the levels of SEAP secreted into the culture medium (Fig. 6). Non-coated stainless steel mesh was used as a control in all transfection experiments with SEAP-DNA. Using plasmid DNA encoding for SEAP allows quantitative and nondestructive determination of transfection over time because the protein is secreted into culture medium.

SEAP expression was measured daily from day 2 until day 12 after cell seeding. The medium was replaced with a fresh cell culture medium at the time of sampling. $(DNA/RHB)_{15}$ films provided higher levels of transgene expression than $(DNA/PEI)_{15}$ in both cell lines tested. In addition, the cumulative transfection activity was about 5-times higher in the faster growing NIH-3T3 cells than in SMC. The duration of the transfection in NIH-3T3 cells from the reducible DNA/RHB was significantly longer than that provided by the non-reducible DNA/PEI films (8 vs. 3 days), suggesting a controlled release of DNA from the reducible films over time. The differences in the total levels and duration of transfection between reducible and non-reducible films can be explained by sustained release of DNA from the reducible films. We hypothesize that the mild reducing microenvironment of plasma membrane of cells growing on the LbL films is responsible for the reduction of disulfide bonds in DNA/RHB films and release of DNA. The molecular weight of RHB is decreased in the process of reduction and this leads to a lower affinity to DNA. The molecular weight of the RHB fragments after full reduction increases with increasing content of the reducible CBA and degree of branching (Scheme 1). The resultant molecular weight is an important parameter that will determine the condensation state of plasmid DNA released from the films. Since the RHB used in this study contains only 33% of the reducible CBA monomer, we expect that the released DNA is at least partially associated with the RHB fragments. These DNA associates are then most likely internalized by the cells via an endocytic process similar to that involved in uptake of soluble polycation/DNA complexes. In comparison, the release of DNA from DNA/PEI films is less efficient due to the lack of a trigger mechanism. It is likely that the initial transfection activity observed in DNA/PEI films is due to loosely associated upper-most layers of DNA and/or DNA/PEI particles on the surface of the films [18]. The trigger used in this study relies on reducing the molecular weight of polycations in the LbL films and subsequent decrease in affinity between the anionic and cationic layers. Other, more efficient, methods of film disassembly have been proposed that rely on complete removal of the charge on polycations or reversal of charge from positive to negative [41-43]. However, considering that polycations, either free or associated with DNA, may play a positive role in mediating cellular

delivery and subcellular trafficking of DNA, it remains to be seen which approach to LbL film disassembly is optimal for gene delivery.

To gain further understanding of the transfection activity of the reducible DNA/RHB, the films were prepared using GFP plasmid DNA and cells expressing GFP were visualized in live cells by fluorescence microscopy (Fig. 7) and in fixed cells by confocal microscopy (Fig. 8). Cell nuclei were stained with the blue Hoechst3342 dye. Comparing the pattern of GFP expression with the nucleus labeling suggests that nearly all cells are transfected and express GFP. Individual GFP expressing cells are clearly visible on the surface of the mesh wire where the cells grow as a monolayer (Fig. 7a), while non-differentiated GFP signal is observed when focusing deeper into the structure between the mesh wires (Fig. 7b). The lack of discrete cell resolution in Fig. 7b is caused by the cells growing in multiple layers. Although majority of cells is GFP positive, we cannot distinguish in these experiments between GFP positive cells that are the result of primary transfection and those that are descendants of those transfected cells. Confocal microscopy was used to allow better separation of the different planes of view not possible with the fluorescence microscopy (Fig. 8). The confocal images confirm the findings of high levels of GFP expression both on the surface of the mesh wires (Fig. 8a) but also high levels of expression in the mesh holes (Fig. 8b). Overall, the transfection results confirm effectiveness of substrate-mediated gene delivery [10,44,45].

3.5. Histology

Subcutaneous implantation of synthetic foreign body materials elicits non-specific protein adsorption and can cause chronic inflammation and other wound healing responses [48-50]. As shown in Fig. 9, the site of implantation healed well after 8 days with no external signs of adverse reaction. On resection of the implanted mesh on day 12, fibrous encapsulation of the mesh was observed for both the control non-coated and $(DNA/RHB)_{15}$ coated sample (Fig. 9b, c). Signs of angiogenesis can also be found in both the coated and non-coated mesh samples.

To further assess the *in vivo* biocompatibility of the control and LbL-coated mesh, the implanted material was removed with the surrounding tissue (Fig. 9d). The tissue samples were fixed in 10% neutral buffered formalin. Sections of the tissue embedded in paraffin were prepared for histological analysis from the tissue located in the immediate vicinity of the implant. The cross-section slices of the tissue surrounding the mesh coated with $(DNA/RHB)_{15}$ (Fig. 10a) and the control non-coated mesh (Fig. 10b) were subjected to hematoxylin and eosin (H&E) staining. The images show no significant variation in the number of macrophages and lymphocytes in the tissue closest to the mesh in both the samples. On average, it appears that more blood vessels were formed in tissue surrounding the non-coated mesh than in tissue around LbL-coated mesh. The fibroblasts create a fibrous capsule, which was imaged by Trichrome stain (Fig. 10c, d). These images confirm that a fibrous capsule formed around the mesh sample within the 12 days. The blue color represents the collagenous fibers that were formed around the mesh. The fibrous capsule was present in both the $(DNA/RHB)_{15}$ coated and uncoated samples. However, it did appear that there were more cell nuclei and increased amounts of collagen fibers around the samples coated with $(DNA/RHB)_{15}$ versus non-coated samples.

3.6. *In vivo* transfection

In vivo transfection activity was evaluated by subcutaneously implanting the stainless steel mesh coated with $(DNA/RHB)_{15}$ films containing SEAP plasmid DNA and measuring the levels of SEAP secreted into the blood circulation of rats (Fig. 11). Non-coated mesh was used in control animals. Blood samples were taken from lateral saphenous vein on the day of mesh implantation and then on days 1, 2, 3, 5, 7, 8, 10, 11, and 12. The blood levels of SEAP peaked on day 5 post-implantation, corresponding to ~160 ng SEAP/mL blood. Assuming 7.1 mL/100

g body weight, the SEAP plasma concentration translates into total plasma SEAP amount ~3.2 μg per animal. The reported half-life of SEAP in blood is ~17 h, which suggests that the plasma levels observed here are the result of sustained transgene expression from the LbL film rather than persistence of SEAP in the plasma [46,47]. As expected, background levels of blood concentration of SEAP were observed when control mesh without DNA was used. Based on the observed high transfection activity of the LbL films in fibroblasts *in vitro* (Fig. 7), we predict that the observed *in vivo* transfection is also most likely due to transfected fibroblasts in the vicinity of the implant. Considering the high DNA doses required for efficient transfection after intravenous injection, it is unlikely that a transfection of a distant organ, such as liver, by systemically distributed DNA released from the LbL film contributes much to the observed levels of SEAP in the plasma. The relatively short duration and sharp decline of the SEAP plasma levels after day 5 may be related to the formation of the fibrous capsule around the LbL implant. It is possible that the collagen in the fibrous capsule created a barrier for efficient diffusion of SEAP from the site of implantation to the blood circulation. Further studies are required to address questions about the levels and duration of transfection as well as type of cells transfected at the site of implantation.

4. CONCLUSION

The study provides a comprehensive evaluation of *in vitro* and *in vivo* DNA delivery from LbL films containing a new class of bioreducible hyperbranched polycations as well as the physical characterization of the LbL films themselves on stainless steel meshes. The most significant conclusion of the study is that RHB-containing LbL films show higher and prolonged transfection than control PEI-containing films *in vitro* and exhibit promising activity *in vivo*. The results fill a gap in understanding biological activity of bioreducible LbL films and suggest that exofacial reducing microenvironment of plasma membrane can indeed serve as a trigger in physiological conditions. These findings demonstrate the potential of the bioreducible LbL films for localized gene delivery applications, such as in regenerative medicine and functional tissue repair and replacement [51].

Acknowledgements

This work was supported by the National Institutes of Health (CA 109711). We thank Pamela VandeVord and Howard Matthews for helpful discussions of the histological data.

References

1. De Laporte L, Shea LD. Matrices and scaffolds for DNA delivery in tissue engineering. Adv Drug Delivery Rev 2007;59:292–307.
2. Chung HJ, Park TG. Surface engineered and drug releasing pre-fabricated scaffolds for tissue engineering. Adv Drug Delivery Rev 2007;59:249–262.
3. Jewell CM, Lynn DM. Multilayered polyelectrolyte assemblies as platforms for the delivery of DNA and other nucleic acid-based therapeutics. Adv Drug Delivery Rev 2008;60:979–999.
4. Hu WW, Wang Z, Hollister SJ, Krebsbach PH. Localized viral vector delivery to enhance in situ regenerative gene therapy. Gene Ther 2007;14:891–901. [PubMed: 17344901]
5. Segura T, Chung PH, Shea LD. DNA delivery from hyaluronic acid-collagen hydrogels via a substrate-mediated approach. Biomaterials 2005;26:1575–1584. [PubMed: 15522759]
6. Shea LD, Smiley E, Bonadio J, Mooney DJ. DNA delivery from polymer matrices for tissue engineering. Nat Biotechnol 1999;17:551–554. [PubMed: 10385318]
7. Luo D, Saltzman WM. Enhancement of transfection by physical concentration of DNA at the cell surface. Nat Biotechnol 2000;18:893–895. [PubMed: 10932162]
8. Shen H, Tan J, Saltzman WM. Surface-mediated gene transfer from nanocomposites of controlled texture. Nat Mater 2004;3:569–574. [PubMed: 15258575]

9. Jewell CM, Zhang J, Fredin NJ, Lynn DM. Multilayered polyelectrolyte films promote the direct and localized delivery of DNA to cells. J Control Release 2005;106:214–223. [PubMed: 15979188]
10. Segura T, Volk MJ, Shea LD. Substrate-mediated DNA delivery: role of the cationic polymer structure and extent of modification. J Control Release 2003;93:69–84. [PubMed: 14602423]
11. Dimitrova M, Arntz Y, Lavalle P, Meyer F, Wolf M, Schuster C, et al. Adenoviral gene delivery from multilayered polyelectrolyte architectures. Adv Funct Mater 2007;17:233–245.
12. Jessel N, Oulad-Abdeighani M, Meyer F, Lavalle P, Haikel Y, Schaaf P, et al. Multiple and time-scheduled in situ DNA delivery mediated by beta-cyclodextrin embedded in a polyelectrolyte multilayer. Proc Natl Acad Sci U S A 2006;103:8618–8621. [PubMed: 16735471]
13. Tang ZY, Wang Y, Podsiadlo P, Kotov NA. Biomedical applications of layer-by-layer assembly: From biomimetics to tissue engineering. Adv Mater 2006;18:3203–3224.
14. Lynn DM. Peeling back the layers: Controlled erosion and triggered disassembly of multilayered polyelectrolyte thin films. Adv Mater 2007;19:4118–4130.
15. De Geest BG, Sanders NN, Sukhorukov GB, Demeester J, De Smedt SC. Release mechanisms for polyelectrolyte capsules. Chem Soc Rev 2007;36:636–649. [PubMed: 17387411]
16. Zhang J, Chua LS, Lynn DM. Multilayered thin films that sustain the release of functional DNA under physiological conditions. Langmuir 2004;20:8015–8021. [PubMed: 15350066]
17. Ren K, Ji J, Shen J. Construction and enzymatic degradation of multilayered poly-l-lysine/DNA films. Biomaterials 2006;27:1152–1159. [PubMed: 16102814]
18. Blacklock J, Handa H, Soundara Manickam D, Mao G, Mukhopadhyay A, Oupicky D. Disassembly of layer-by-layer films of plasmid DNA and reducible TAT polypeptide. Biomaterials 2007;28:117–124. [PubMed: 16962657]
19. Saito G, Swanson JA, Lee KD. Drug delivery strategy utilizing conjugation via reversible disulfide linkages: role and site of cellular reducing activities. Adv Drug Delivery Rev 2003;55:199–215.
20. Manickam SD, Oupicky D. Polyplex gene delivery modulated by redox potential gradients. J Drug Targeting 2006;14:519–526.
21. Zelikin AN, Li Q, Caruso F. Degradable polyelectrolyte capsules filled with oligonucleotide sequences. Angew Chem Int Ed Engl 2006;45:7743–7745. [PubMed: 17075936]
22. Zelikin AN, Quinn JF, Caruso F. Disulfide cross-linked polymer capsules: En route to biodeconstructible systems. Biomacromolecules 2006;7:27–30. [PubMed: 16398494]
23. Haynie DT, Palath N, Liu Y, Li BY, Pargaonkar N. Biomimetic nanostructured materials: Inherent reversible stabilization of polypeptide microcapsules. Langmuir 2005;21:1136–1138. [PubMed: 15667201]
24. Kichler A, Remy JS, Boussif O, Frisch B, Boeckler C, Behr JP, et al. Efficient Gene Delivery with Neutral Complexes of Lipospermine and Thiol-Reactive Phospholipids. Biochem Biophys Res Commun 1995;209:444–450. [PubMed: 7733911]
25. Jones DP, Carlson JL, Samiec PS, Sternberg P Jr, Mody VC Jr, Reed RL, et al. Glutathione measurement in human plasma. Evaluation of sample collection, storage and derivatization conditions for analysis of dansyl derivatives by HPLC. Clin Chim Acta 1998;275:175–184. [PubMed: 9721075]
26. Ryser HJ, Mandel R, Ghani F. Cell surface sulfhydryls are required for the cytotoxicity of diphtheria toxin but not of ricin in Chinese hamster ovary cells. J Biol Chem 1991;266:18439–18442. [PubMed: 1655751]
27. Feener EP, Shen WC, Ryser HJP. Cleavage of Disulfide Bonds in Endocytosed Macromolecules - a Processing Not Associated With Lysosomes or Endosomes. J Biol Chem 1990;265:18780–18785. [PubMed: 2229041]
28. Sahaf B, Heydari K, Herzenberg LA, Herzenberg LA. The extracellular microenvironment plays a key role in regulating the redox status of cell surface proteins in HIV-infected subjects. Arch Biochem Biophys 2005;434:26–32. [PubMed: 15629105]
29. Donoghue N, Hogg PJ. Characterization of redox-active proteins on cell surface. Methods Enzymol 2002;348:76–86. [PubMed: 11885296]
30. Gilbert HF. Protein disulfide isomerase and assisted protein folding. J Biol Chem 1997;272:29399–29402. [PubMed: 9367991]

31. Donoghue N, Yam PTW, Jiang XM, Hogg PJ. Presence of closely spaced protein thiols on the surface of mammalian cells. Protein Sci 2000;9:2436–2445. [PubMed: 11206065]
32. Jiang XM, Fitzgerald M, Grant CM, Hogg PJ. Redox control of exofacial protein thiols/disulfides by protein disulfide isomerase. J Biol Chem 1999;274:2416–2423. [PubMed: 9891011]
33. Laragione T, Bonetto V, Casoni F, Massignan T, Bianchi G, Gianazza E, et al. Redox regulation of surface protein thiols: identification of integrin alpha-4 as a molecular target by using redox proteomics. Proc Natl Acad Sci U S A 2003;100:14737–14741. [PubMed: 14657342]
34. Lin C, Zhong Z, Lok MC, Jiang X, Hennink WE, Feijen J, et al. Linear poly(amido amine)s with secondary and tertiary amino groups and variable amounts of disulfide linkages: synthesis and in vitro gene transfer properties. J Control Release 2006;116:130–137. [PubMed: 17079046]
35. Hoon Jeong J, Christensen LV, Yockman JW, Zhong Z, Engbersen JF, Jong Kim W, et al. Reducible poly(amido ethylenimine) directed to enhance RNA interference. Biomaterials 2007;28:1912–1917. [PubMed: 17218006]
36. Christensen LV, Chang CW, Kim WJ, Kim SW, Zhong ZY, Lin C, et al. Reducible poly(amido ethylenimine)s designed for triggered intracellular gene delivery. Bioconjugate Chem 2006;17:1233–1240.
37. Wu DC, Liu Y, Chen L, He CB, Chung TS, Goh SH. 2A(2)+BB ’ B ” approach to hyperbranched poly(amino ester)s. Macromolecules 2005;38:5519–5525.
38. Jewell CM, Zhang J, Fredin NJ, Wolff MR, Hacker TA, Lynn DM. Release of plasmid DNA from intravascular stents coated with ultrathin multilayered polyelectrolyte films. Biomacromolecules 2006;7:2483–2491. [PubMed: 16961308]
39. Meyer F, Dimitrova M, Jedrzejenska J, Arntz Y, Schaaf P, Frisch B, et al. Relevance of bi-functionalized polyelectrolyte multilayers for cell transfection. Biomaterials 2008;29:618–624. [PubMed: 17996296]
40. Boulange-Petermann L, Doren A, Baroux B, Bellon-Fontaine MN. Zeta potential measurements on passive metals. J Colloid Interface Sci 1995;171:179–186.
41. Zhang JT, Lynn DM. Ultrathin multilayered films assembled from “Charge-Shifting” cationic polymers: Extended, long-term release of plasmid DNA from surfaces. Adv Mater 2007;19:4218–+.
42. Luten J, Akeroyd N, Funhoff A, Lok MC, Talsma H, Hennink WE. Methacrylamide polymers with hydrolysis-sensitive cationic side groups as degradable gene carriers. Bioconjugate Chem 2006;17:1077–1084.
43. Liu X, Yang JW, Lynn DM. Addition of “charge-shifting” side chains to linear poly(ethyleneimine) enhances cell transfection efficiency. Biomacromolecules 2008;9:2063–2071. [PubMed: 18564876]
44. Bengali Z, Pannier AK, Segura T, Anderson BC, Jang JH, Mustoe TA, et al. Gene delivery through cell culture substrate adsorbed DNA complexes. Biotechnol Bioeng 2005;90:290–302. [PubMed: 15800863]
45. Segura T, Shea LD. Surface-tethered DNA complexes for enhanced gene delivery. Bioconjug Chem 2002;13:621–629. [PubMed: 12009954]
46. Chastain M, Simon AJ, Soper KA, Holder DJ, Montgomery DL, Sagar SL, et al. Antigen levels and antibody titers after DNA vaccination. J Pharm Sci 2001;90:474–484. [PubMed: 11170037]
47. Kwok KY, Park Y, Yang Y, McKenzie DL, Liu Y, Rice KG. In vivo gene transfer using sulfhydryl cross-linked PEG-peptide/glycopeptide DNA co-condensates. J Pharm Sci 2003;92:1174–1185. [PubMed: 12761807]
48. Ratner BD, Bryant SJ. BIOMATERIALS: Where We Have Been and Where We are Going. Annu Rev Biomed Eng 2004;6:41–75. [PubMed: 15255762]
49. Anderson JM. Biological responses to materials. Annu Rev Mater Res 2001;31:81–110.
50. Keselowsky BG, Bridges AW, Burns KL, Tate CC, Babensee JE, LaPlaca MC, et al. Role of plasma fibronectin in the foreign body response to biomaterials. Biomaterials 2007;28:3626–3631. [PubMed: 17521718]
51. Pannier AK, Shea LD. Controlled release systems for DNA delivery. Mol Ther 2004;10:19–26. [PubMed: 15233938]

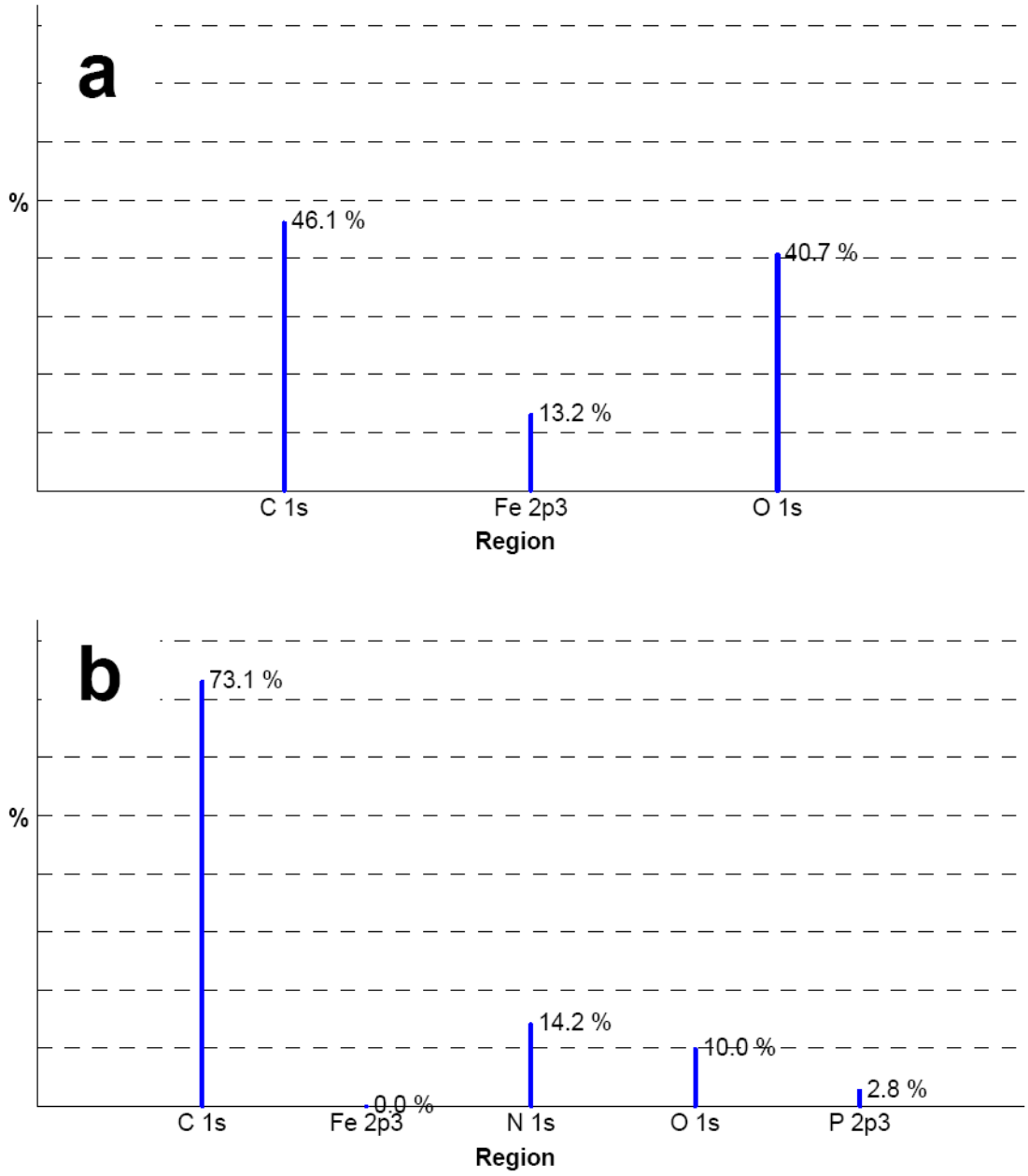

Figure 1.
Surface characterization of DNA/RHB films. XPS spectra of non-coated stainless steel mesh (a) and stainless steel mesh coated with $(DNA/RHB)_{15}$ film.

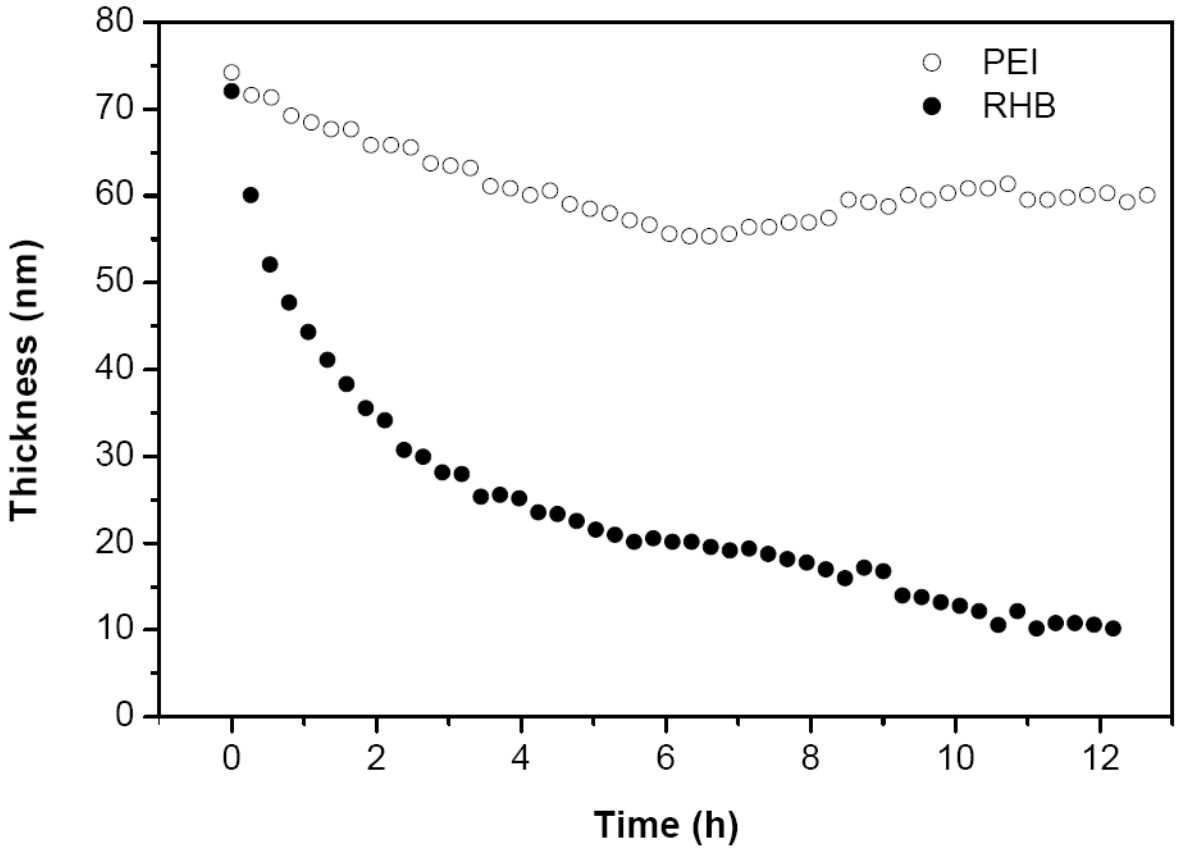

Figure 2.
Film disassembly in reducing conditions. Thickness of $(DNA/RHB)_{15}$ (●) and $(DNA/PEI)_{15}$ (○) films deposited on the surface of silicon wafer was monitored by ellipsometry in 20 mM DTT solution.

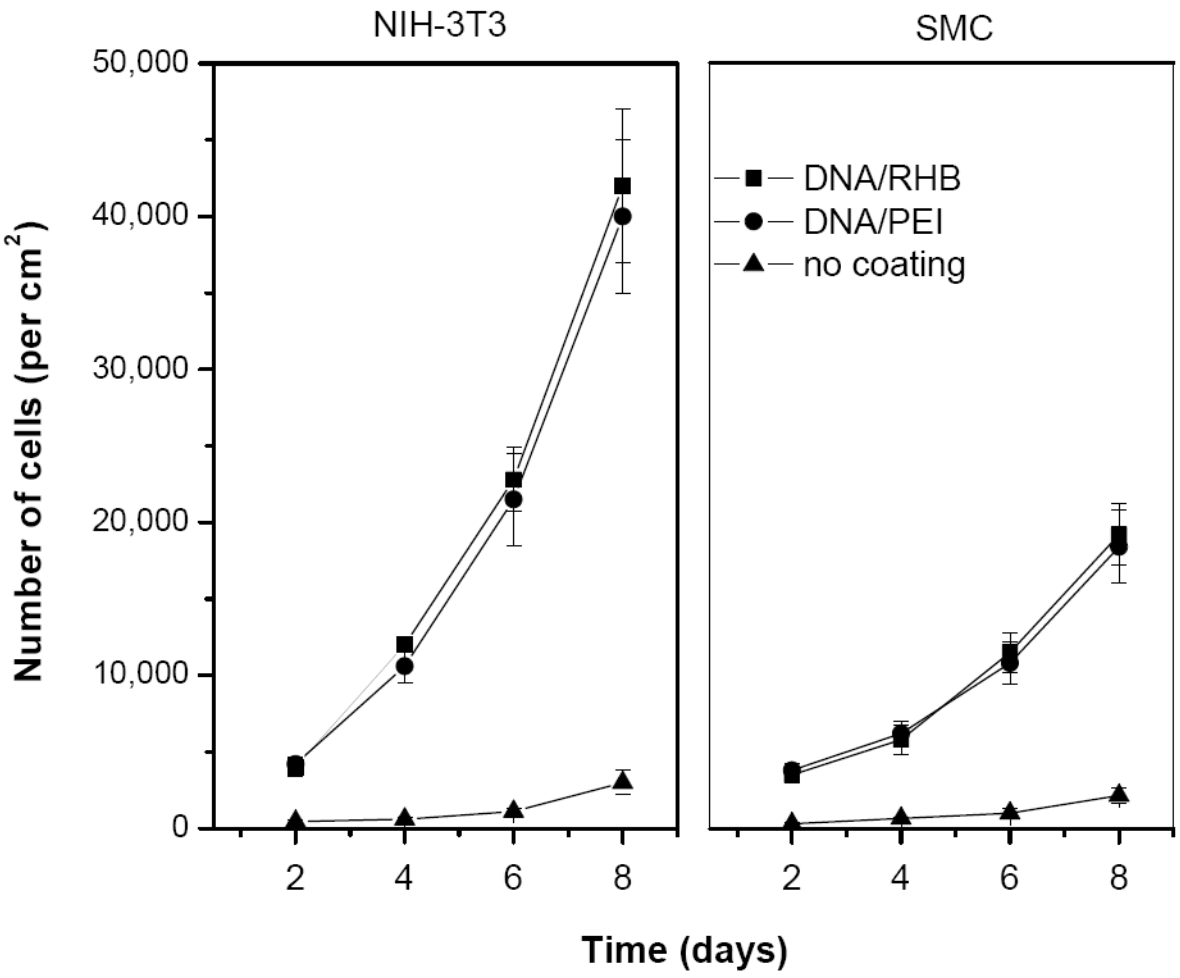

Figure 3.

Cell proliferation on stainless steel mesh coated with LbL films. Growth of NIH-3T3 (left panel) and SMC (right panel) was followed by measuring LDH content in cell lysates from the mesh coated with $(DNA/RHB)_{15}$ (■) or $(DNA/PEI)_{15}$ (●). Control non-coated mesh (▲). Results are expressed as mean number of cells/cm^2 mesh ± SD of triplicate samples.

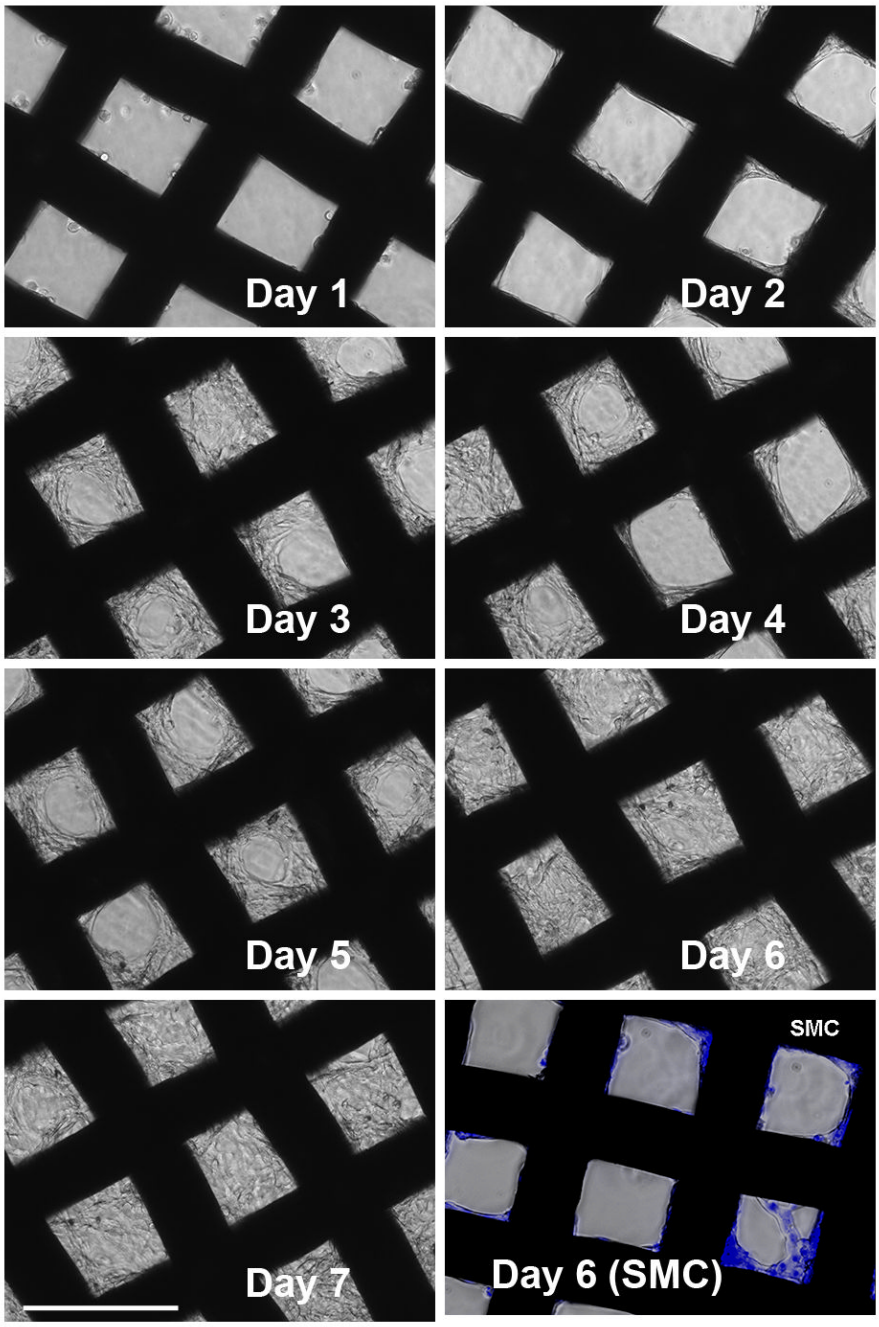

Figure 4.
Cell growth pattern on $(DNA/RHB)_{15}$ films. NIH-3T3 cells were imaged daily by optical microscopy. Bottom right panel shows SMC imaged 6 days after cell seeding (nuclei stained with Hoechst3342). (size bar = 200 μm)

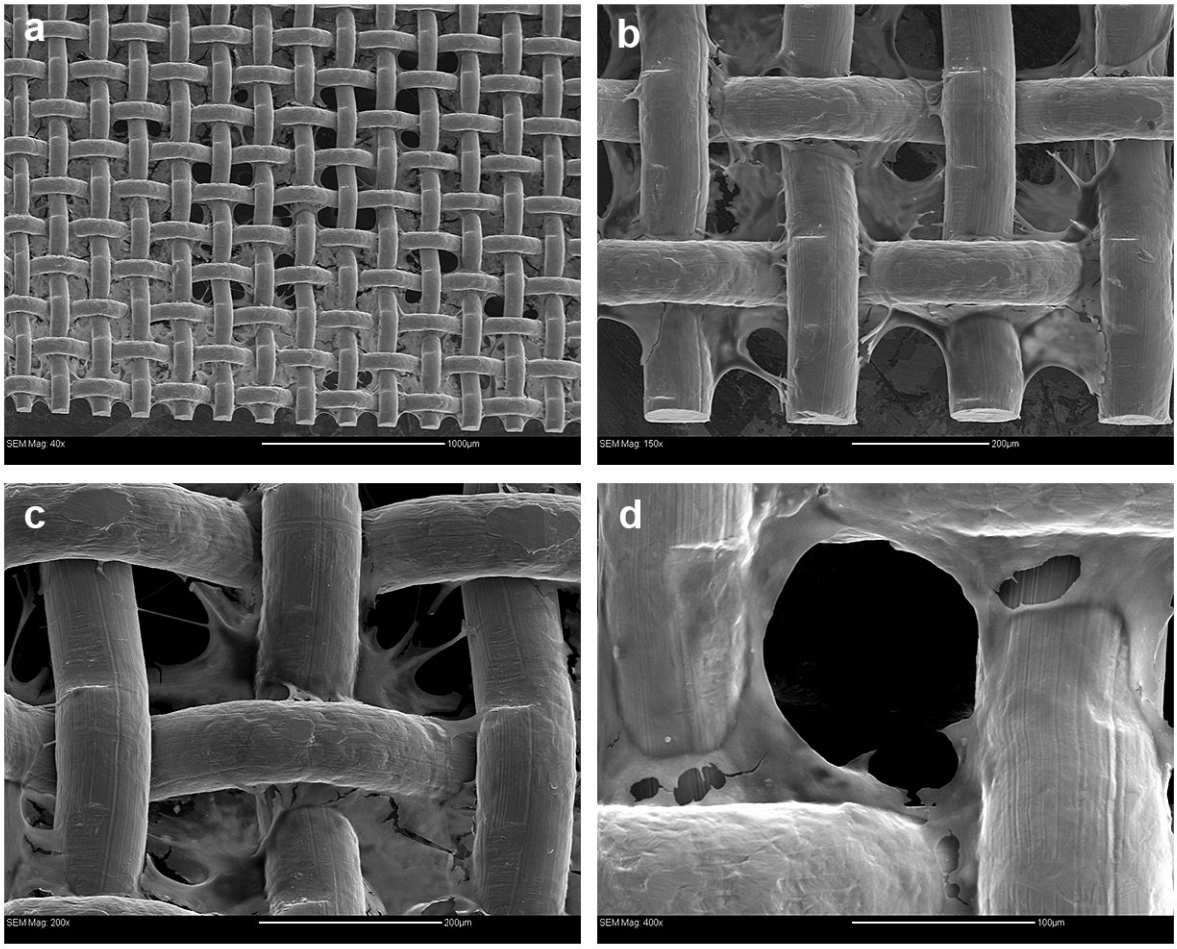

Figure 5.
SEM images of NIH-3T3 cells 6 days after cell seeding on $(DNA/RHB)_{15}$ film. Magnification and bar size (a) 40×, 200 μm; (b) 150×, 1000 μm; (c) 200×, 200 μm; (d) 400×, 100 μm.

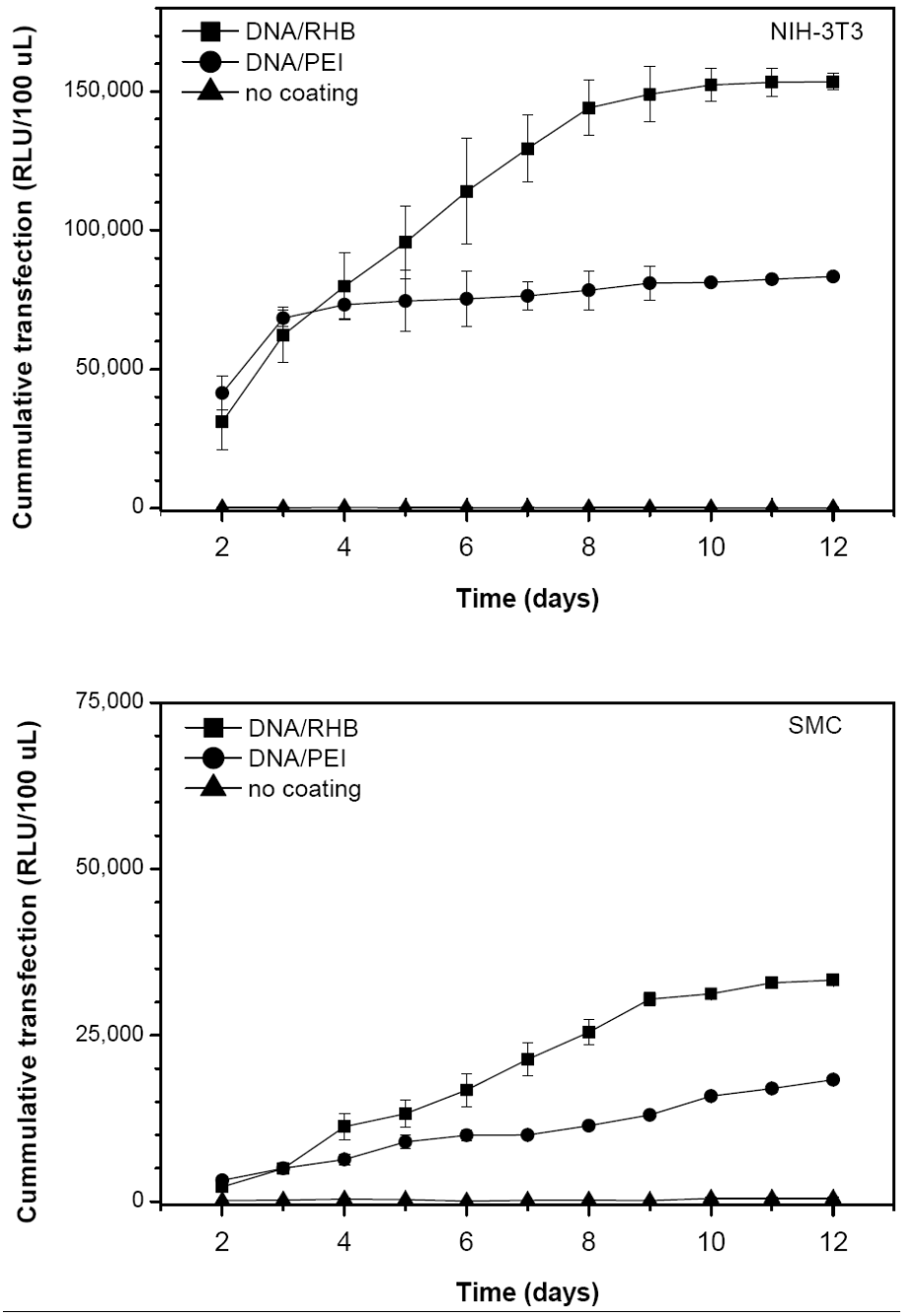

Figure 6.

Transfection activity of LbL films based on SEAP-DNA. Stainless steel mesh coated with $(DNA/RHB)_{15}$ (■), $(DNA/PEI)_{15}$ (●), and control non-coated mesh (▲) were used to transfect NIH-3T3 (a) and SMC (b) cells. Cumulative levels of SEAP expression are expressed as mean relative light units (RLU/100 μL) ± SD (n = 3).

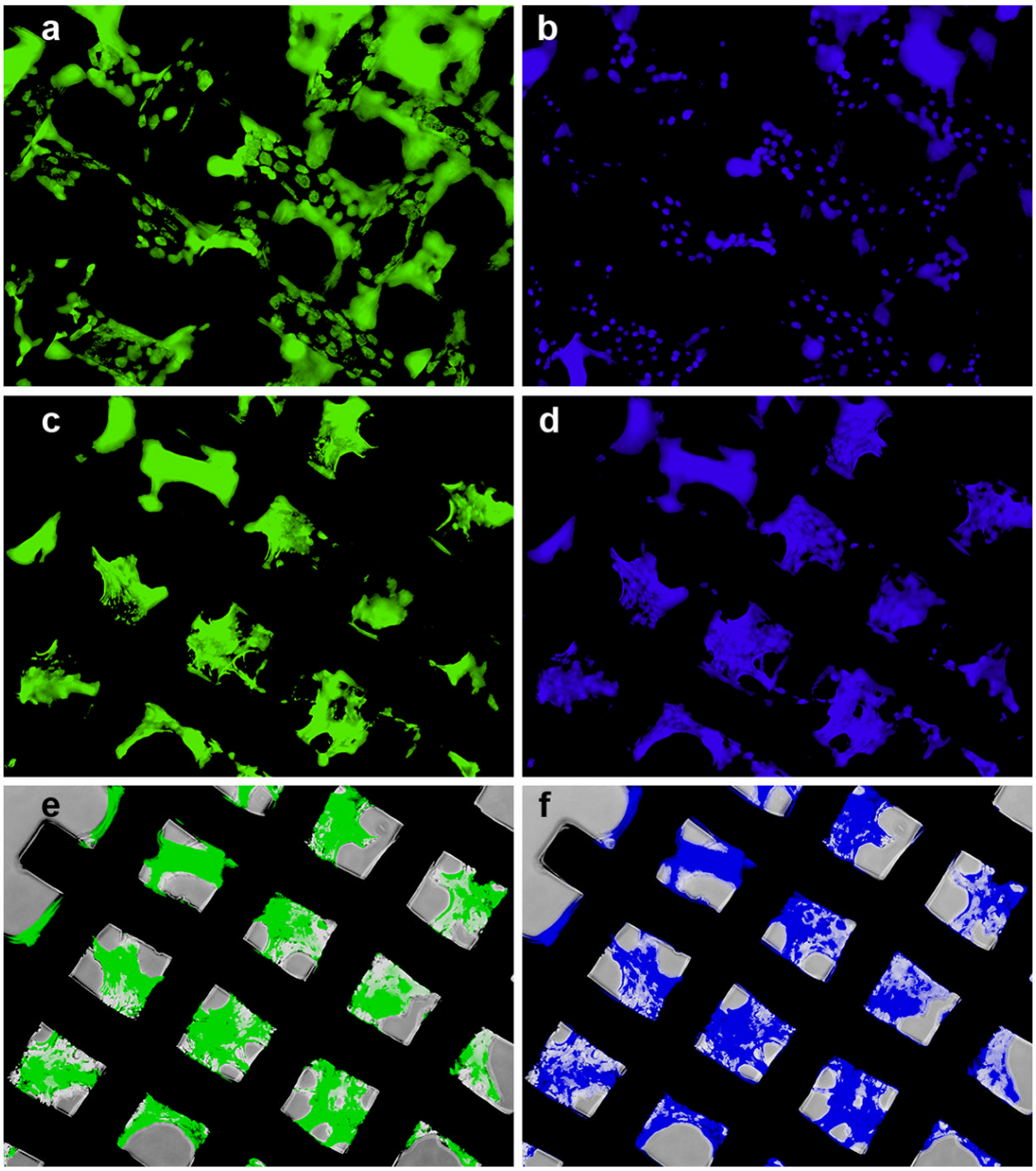

Figure 7.
Transfection activity of $(DNA/RHB)_{15}$ films based on GFP-DNA. Fluorescence microscopy images of GFP expression in NIH-3T3 cells with the plane of focus on top of the mesh wires (a) and in spaces between the wires (c). Corresponding images of cells with nuclei stained with Hoechst3342 (b, d). Phase and fluorescence overlay (e, f).

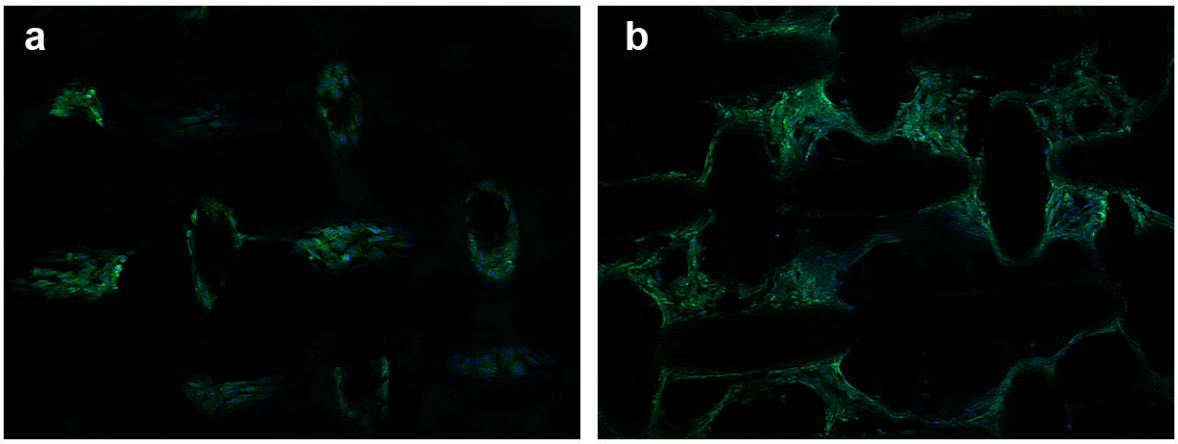

Figure 8.

Confocal microscopy images of NIH-3T3 cells transfected with $(DNA/RHB)_{15}$ films based on GFP-DNA. Overlay images of GFP expression and cell nuclei stained with Hoechst3342 with the plane of focus on top of the mesh wires (a) and in spaces between the wires (c). (20× magnification)

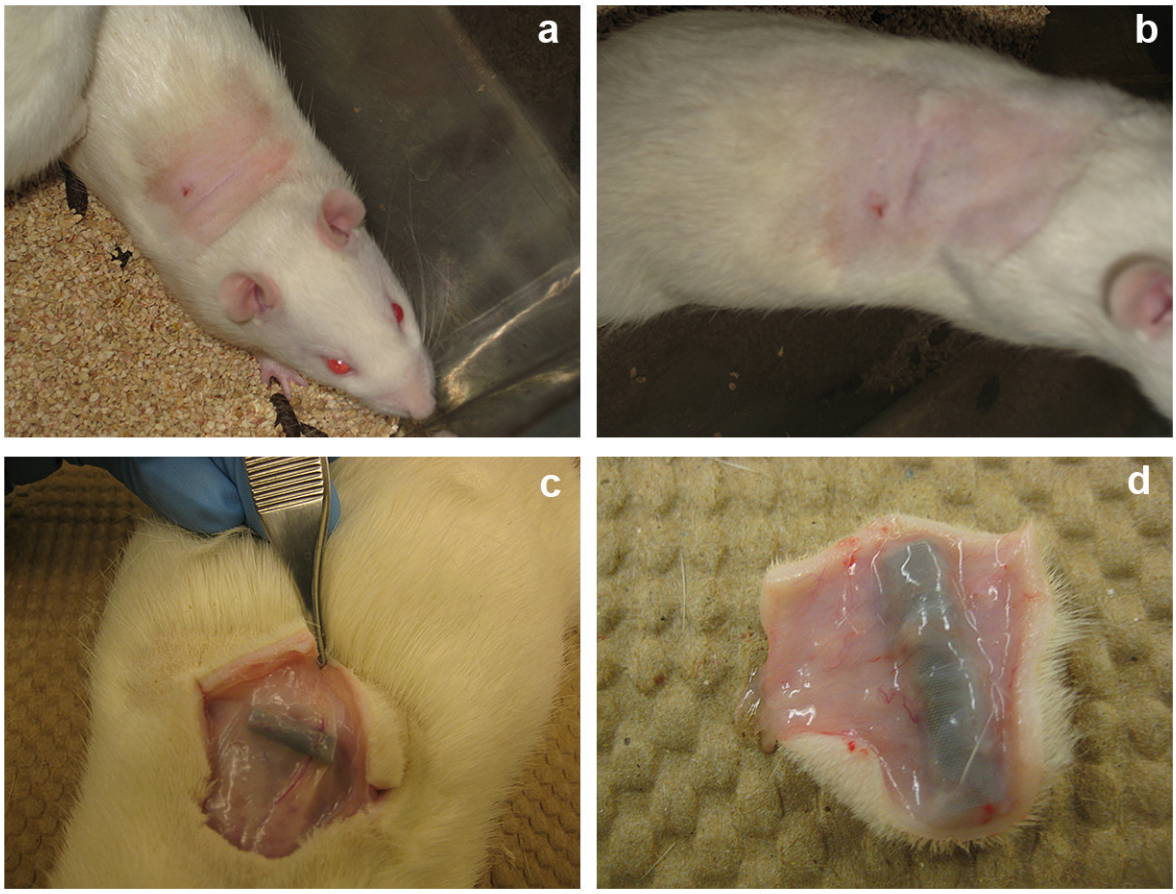

Figure 9.
Implant excision. Healed wound observed 8 days after implantation of steel mesh coated with $(DNA/RHB)_{15}$ films (a, b). Implant excision on day 12 (c, d).

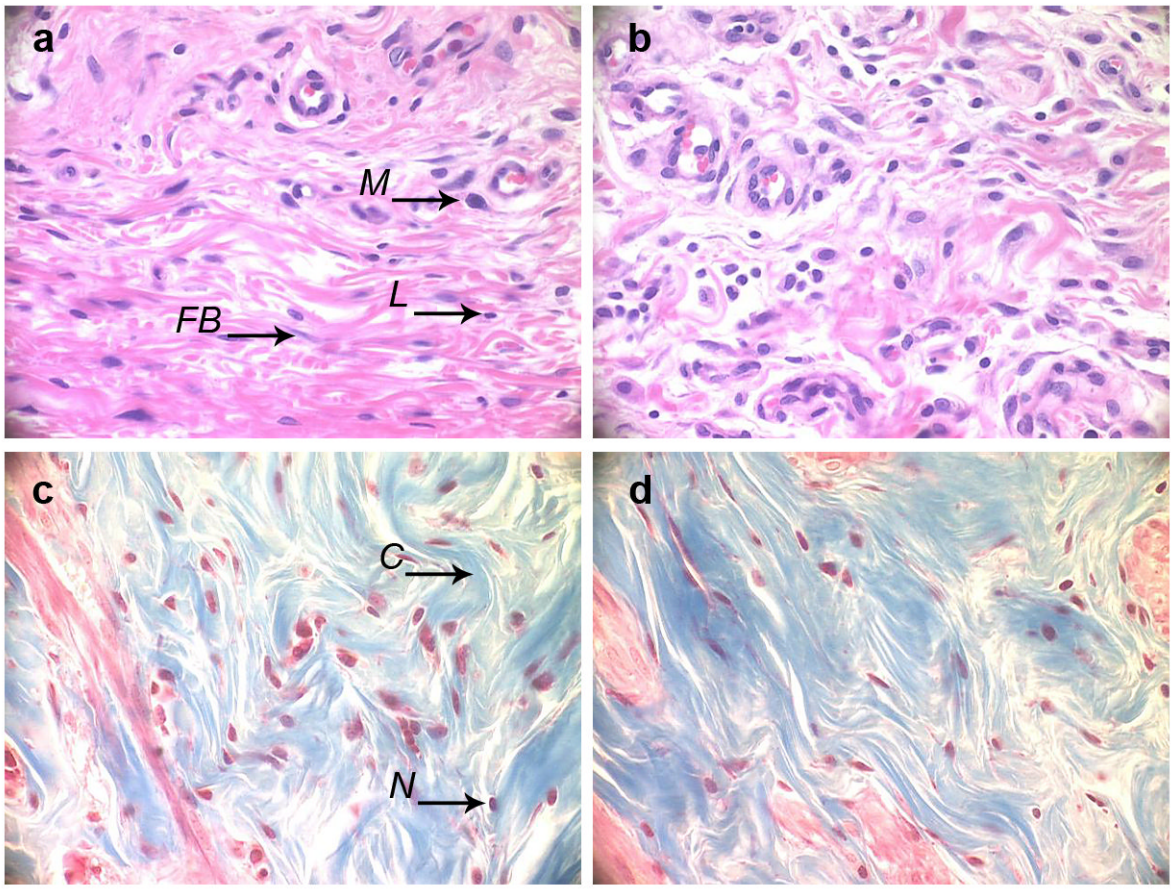

Figure 10.
Histological analysis. H&E (a, b) and Trichrome (c, d) stains of the section of tissue adjacent to the stainless steel mesh implant coated with $(DNA/RHB)_{15}$ films (a, c) and control non-coated mesh (b, d). (M – macrophage, FB – fibroblast, L – lymphocyte, C – collagen, N – cell nucleus). (all images at 40× magnification, implant/tissue interface at the top of the images)

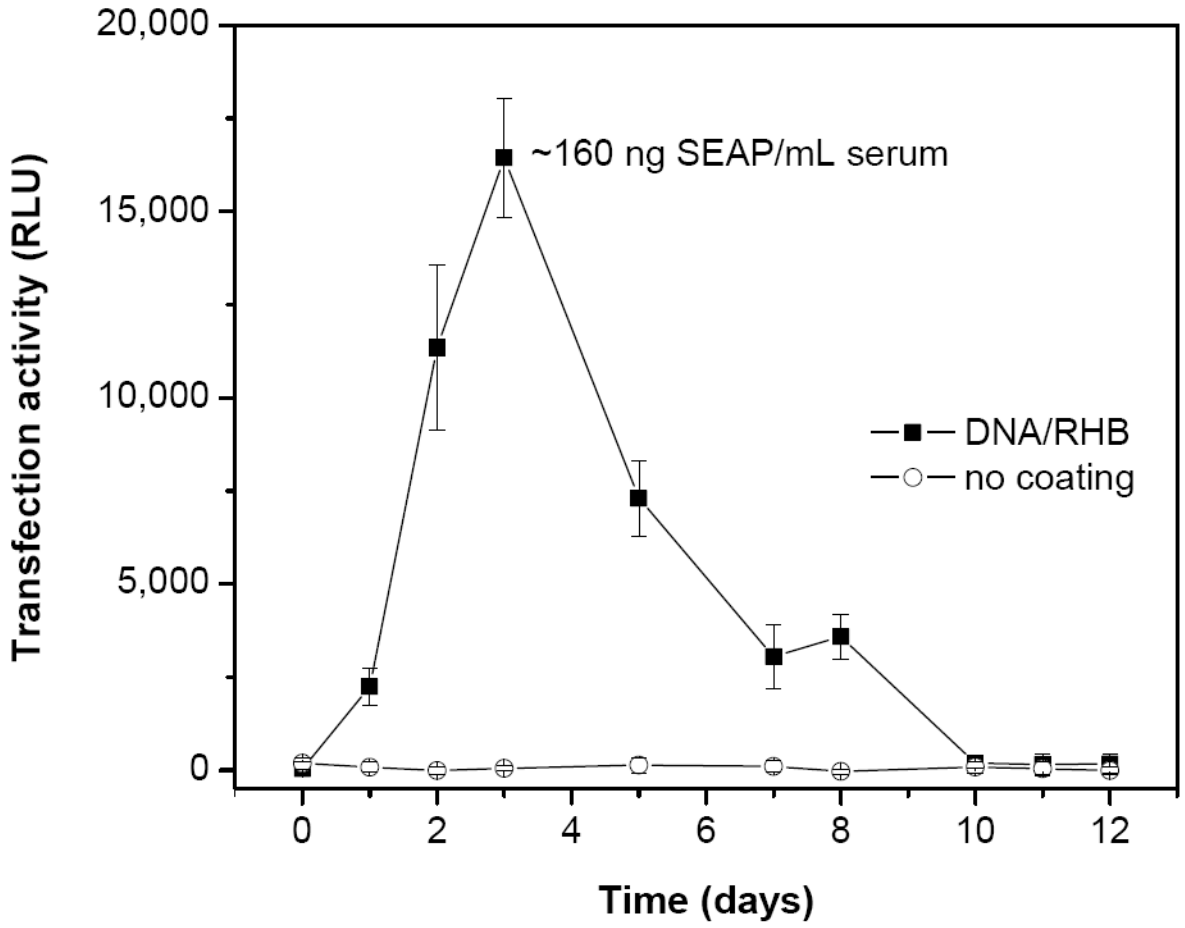

Figure 11.

In vivo transfection activity of $(DNA/RHB)_{15}$ films. Stainless steel mesh coated with $(DNA/RHB)_{15}$ (■) and control non-coated mesh (○) were implanted subcutaneously in rats and levels of SEAP expression in blood plasma were measured. Transfection is expressed as mean relative light units (RLU) ± SD (n = 6).

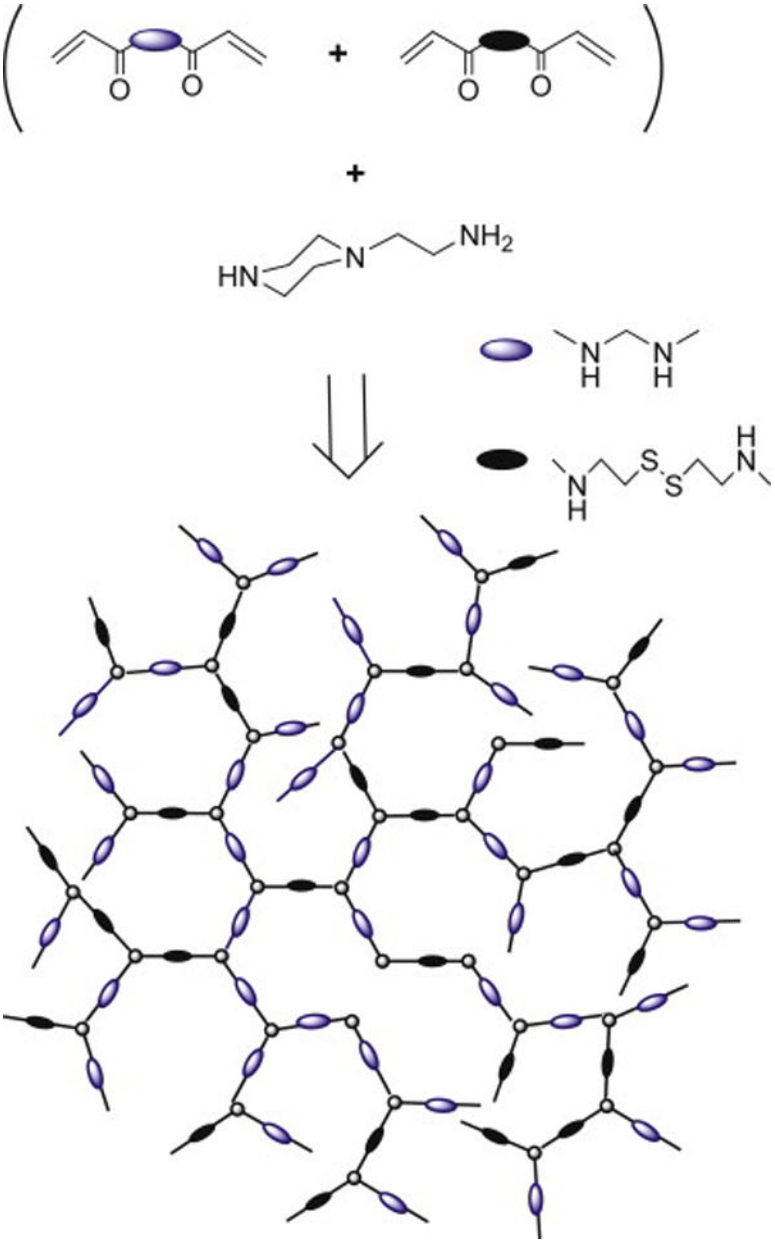

Scheme 1.
Synthesis of reducible hyperbranched poly(amido amine) (RHB).